J|A|C|S
ARTICLES

Published on Web 08/22/2008

Structure, Magnetism, and Theoretical Study of a Mixed-Valence $Co^{II}_3Co^{III}_4$ Heptanuclear Wheel: Lack of SMM Behavior despite Negative Magnetic Anisotropy

Liviu F. Chibotaru,*,† Liviu Ungur,† Christophe Aronica,‡ Hani Elmoll,‡
Guillaume Pilet,‡ and Dominique Luneau*,‡

Afdeling Kwantumchemie en Fysicochemie, Katholieke Universiteit Leuven,
Celestijnenlaan 200F, B-3001 Leuven, Belgium, and Université Claude Bernard Lyon 1,
Laboratoire des Multimatériaux et Interfaces (UMR 5615), Campus de La Doua,
69622 Villeurbanne Cedex, France

Received April 21, 2008; E-mail: Liviu.Chibotaru@chem.kuleuven.be; luneau@univ-lyon1.fr

Abstract: A mixed-valence Co(II)/Co(III) heptanuclear wheel $[Co^{II}_3Co^{III}_4(L)_6(MeO)_6]$ (LH_2 = 1,1,1-trifluoro-7-hydroxy-4-methyl-5-aza-hept-3-en-2-one) has been synthesized and its crystal structure determined using single-crystal X-ray diffraction. The valence state of each cobalt ion was established by bond valence sum calculations. Studies of the temperature dependence of the magnetic susceptibility and the field dependence of the magnetization evidence ferromagnetic interactions within the compound. In order to understand the magnetic properties of this Co_7 wheel, we performed ab initio calculations for each cobalt fragment at the CASSCF/CASPT2 level, including spin−orbit coupling effects within the SO-RASSI approach. The four Co(III) ions were found to be diamagnetic and to give a significant temperature-independent paramagnetic contribution to the susceptibility. The spin−orbit coupling on the three Co(II) sites leads to separations of $\sim$200 cm^{-1} between the ground and excited Kramers doublets, placing the Co_7 wheel into a weak-exchange limit in which the lowest electronic states are adequately described by the anisotropic exchange interaction between the lowest Kramers doublets on Co(II) sites. Simulation of the exchange interaction was done within the Lines model, keeping the fully ab initio treatment of magnetic anisotropy effects on individual cobalt fragments using a recently developed methodology. A good description of the susceptibility and magnetization was obtained for nearest-neighbor (J_1) and next-nearest-neighbor (J_2) exchange parameters (1.5 and 5.5 cm^{-1}, respectively). The strong ferromagnetic interaction between distant cobalt ions arises as a result of low electron-promotion energies in the exchange bridges containing Co(III) ions. The calculations showed a large value of the magnetization along the main magnetic axis (10.1μ_B), which is a combined effect of the ferromagnetic exchange interaction and negative magnetic anisotropy on the two marginal Co(II) sites. The lack of single-molecule magnet behavior in $[Co^{II}_3Co^{III}_4(L)_6(MeO)_6]$ is explained by relatively large matrix elements of transverse magnetic moments between states of maximal magnetization of the ground Kramers doublet, evidenced by ab initio calculations, and the associated large tunneling rates between these states in the presence of dipolar transverse magnetic fields in the crystal.

Introduction

Paramagnetic compounds have been investigated for a long time because of their interesting magnetochemical, catalytic, and physical properties. Recently, high-spin metal complexes have attracted much attention for their exceptional magnetic properties:[1] some of them show slow magnetic relaxation of spin-flipping along the axis of magnetic anisotropy and have been called single-molecule magnets (SMMs).[2−4] The first SMM, discovered in 1991, was an oxo-manganese cluster with a Mn_{12} core.[5] Since then, several types of SMM have been reported, and the field is rapidly expanding.[6,7] Large organic−metal clusters have recently been synthesized, raising the hopes that permanent magnets on the border between mesoscopic and macroscopic systems will soon be created.[7] In order to have a high barrier for reversal of magnetization, an SMM must fulfill two basic requirements:[1,8] it must possess a large ground-state spin (S) and a large negative value of the axial anisotropy parameter (D) in this state. These two factors combine to give the energy of the barrier for reversal of magnetization as follows:[9]

---

† Katholieke Universiteit Leuven.

‡ Université Claude Bernard Lyon 1.

(1) (a) Christou, G.; Gatteschi, D.; Hendrickson, D. N.; Sessoli, R. *MRS Bull.* **2000**, *25*, 66. (b) Gatteschi, D.; Sessoli, R. *Angew. Chem., Int. Ed.* **2003**, *42*, 268–297.

(2) Sessoli, R.; Gatteschi, D.; Caneschi, A.; Novak, M. *Nature* **1993**, *365*, 149.

(3) Oshio, H.; Nihei, M.; Koizumi, S.; Shiga, T.; Nojiri, H.; Nakano, M.; Shirakawa, N.; Akatsu, M. *J. Am. Chem. Soc.* **2005**, *127*, 4568–4569.

(4) Friedman, J. R.; Sarachik, M. P.; Tejada, J.; Ziolo, R. *Phys. Rev. Lett.* **1996**, *76*, 3830.

(5) Caneschi, A.; Gatteschi, D.; Sessoli, R. *J. Am. Chem. Soc.* **1991**, *113*, 5873–5874.

(6) Gatteschi, D.; Sessoli, R.; Cornia, A. *Chem. Commun.* **2000**, 725–732.

(7) Ritter, S. K. *Chem. Eng. News* **2004**, *82*, 29–32.

(8) Oshio, H.; Nakano, M. *Chem.—Eur. J.* **2005**, *11*, 5178–5185.

10.1021/ja8029416 CCC: $40.75 © 2008 American Chemical Society

$$E_{\text{barrier}} = DS^2 \qquad (1)$$

The effective anisotropy parameter D represents the joint contribution of the single-ion anisotropies of all of the magnetic ions entering the complex and their anisotropic magnetic interactions. It should be noted that this interpretation of the height of the barrier for reversal of magnetization is generally valid only in the strong-exchange limit.[10] In this limit, the exchange interactions in the complex lead to separations between low-lying spin-exchange multiplets that are larger than the energy effects of the anisotropic magnetic interactions. As a result, the latter merely split each spin level into several components. This is basically the case for Mn_{12} and for most of the complexes exhibiting SMM behavior that have been investigated to date.[1,11]

On the other hand, in the weak-exchange limit,[10] the magnetic anisotropies on metal sites are much stronger than the exchange interactions between the sites. In this limit, eq 1 is not applicable to the description of the barrier for reversal of magnetization, since it involves the total spin S of the complex, which is no longer a good quantum number. Such a situation is encountered in complexes involving transition-metal ions with strong magnetic anisotropies, such as Co(II), and in almost all complexes involving lanthanides (Ln). Recently, such complexes have started to attract much attention, and some of them have indeed shown SMM or single-chain magnet behavior.[12−23] In these complexes, the ionic anisotropy and the exchange interaction can both contribute to the height of the barrier for reversal of magnetization. The first mechanism alone is responsible for the SMM effect in the mononuclear bis(phthalocyaninato)holmium anion.[23] The pure exchange contribution to the barrier was predicted for some complexes of axial symmetry involving heptacyanomolybdenum(III).[24] In the general case, however, the origin of SMM behavior of complexes in the weak-exchange limit is difficult to elucidate.

The present work addresses such questions. The goal was to investigate the possibility of blockage of magnetization in a mixed-valence Co(II)/Co(III) heptanuclear wheel that we obtained in the course of our work with the ligand 1,1,1-trifluoro-7-hydroxy-4-methyl-5-aza-hept-3-en-2-one (LH_2) whose structure is shown in Scheme 1.[13,25]

Scheme 1. Structure of the LH_2 Ligand

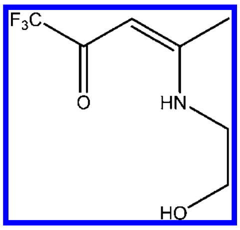

We recently reported tetranuclear and nonanuclear Cu−Ln mixed complexes with this ligand that have cubane-like frameworks.[13,25] Some of these complexes exhibited SMM behavior.[13] In a continuation of this work, in order to find new SMM compounds, we also tried to form complexes of this ligand with Co(II). Indeed, as mentioned above, Co(II) is a good candidate to instill anisotropy, and several Co(II) polynuclear complexes that show SMM properties have been reported.[26−30] The Co(II) complexes are characterized by high anisotropy and a strong orbital contribution to the magnetic moment, in both tetrahedral and octahedral environments.[31] We have reported, for example, a dinuclear complex of tetrahedral Co(II) showing strong negative anisotropies of the Co(II) ions.[32] In the case of Co(II), the reaction with LH_2 in methanol under an aerobic atmosphere afforded a heptanuclear system that was found to be mixed-valent: $[Co^{II}_3Co^{III}_4(L)_6(MeO)_6]$. Although the measured magnetic susceptibility evidenced the overall predominance of ferromagnetic interactions between magnetic centers, Micro-SQUID measurements on single crystals have shown that this heptanuclear complex was not an SMM. Recently, however, heptanuclear manganese[33] and cobalt[34] wheels with similar core structures that do show SMM behavior have been synthesized and investigated.

In this work, using a recently developed ab initio-based methodology for the calculation of magnetic properties of complexes,[35] we were able to rationalize the magnetic data of this complicated system. In particular, we found an explanation for why the investigated complex does not display SMM behavior despite having a ferromagnetic ground state and

---

(9) We note that D and S are not completely independent parameters, since for given local anisotropies on metal sites and anisotropic magnetic interactions between them, D scales as $1/S^2$ (see: Waldmann, O. *Inorg. Chem.* **2007**, *46*, 10035–10037.). However, for a given S, D roughly scales with the number of magnetic metal ions in the case when local anisotropy contributions dominate.

(10) Bencini, A.; Gatteschi, D. *EPR of Exchange Coupled Systems*; Springer: Berlin, 1990.

(11) Aromi, G.; Brechin, E. K. *Struct. Bonding (Berlin)* **2006**, *122*, 1–67.

(12) Andres, H.; Basler, R.; Guedel, H.-U.; Aromi, G.; Christou, G.; Buettner, H.; Ruffle, B. *J. Am. Chem. Soc.* **2000**, *122*, 12469–12477.

(13) Aronica, C.; Pilet, G.; Chastanet, G.; Wernsdorfer, W.; Jacquot, J.-F.; Luneau, D. *Angew. Chem., Int. Ed.* **2006**, *45*, 4659–4662.

(14) Aubin, S. M. J.; Wemple, M. W.; Adams, D. M.; Tsai, H.-L.; Christou, G.; Hendrickson, D. N. *J. Am. Chem. Soc.* **1996**, *118*, 7746–7754.

(15) Barra, A.-L.; Debrunner, P.; Gatteschi, D.; Schulz, C. E.; Sessoli, R. *Europhys. Lett.* **1996**, *35*, 133–138.

(16) Boca, R. *Coord. Chem. Rev.* **2004**, *248*, 757–815.

(17) Castro, S. L.; Sun, Z.; Grant, C. M.; Bollinger, J. C.; Hendrickson, D. N.; Christou, G. *J. Am. Chem. Soc.* **1998**, *120*, 2365–2375.

(18) Gatteschi, D.; Barra, A. L.; Caneschi, A.; Cornia, A.; Sessoli, R.; Sorace, L. *Coord. Chem. Rev.* **2006**, *250*, 1514–1529.

(19) Gatteschi, D.; Sorace, L. *J. Solid State Chem.* **2001**, *159*, 253–261.

(20) Lescouezec, R.; Toma, L. M.; Vaissermann, J.; Verdaguer, M.; Delgado, F. S.; Ruiz-Perez, C.; Lloret, F.; Julve, M. *Coord. Chem. Rev.* **2005**, *249*, 2691–2729.

(21) Rogez, G. *Angew. Chem., Int. Ed.* **2005**, *44*, 1876–1879.

(22) Westin, L. G.; Kritikos, M.; Caneschi, A. *Chem. Commun.* **2003**, 1012–1013.

(23) Ishikawa, N.; Sugita, M.; Wernsdorfer, W. *J. Am. Chem. Soc.* **2005**, *127*, 3650–3651.

(24) Mironov, V. S.; Chibotaru, L. F.; Ceulemans, A. *J. Am. Chem. Soc.* **2003**, *125*, 9750–9760.

(25) Aronica, C.; Chastanet, G.; Pilet, G.; Le Guennic, B.; Robert, V.; Wernsdorfer, W.; Luneau, D. *Inorg. Chem.* **2007**, *46*, 6108–6119.

(26) Brechin, E. K.; Cador, O.; Caneschi, A.; Cadiou, C.; Harris, S. G.; Parsons, S.; Vonci, M.; Winpenny, R. E. P. *Chem. Commun.* **2002**, 1860–1861.

(27) Langley, S. J.; Helliwell, M.; Sessoli, R.; Rosa, P.; Wernsdorfer, W.; Winpenny, R. E. P. *Chem. Commun.* **2005**, 5029–5031.

(28) Moragues-Canovas, M.; Talbot-Eeckelaers, C. E.; Catala, L.; Lloret, F.; Wernsdorfer, W.; Brechin, E. K.; Mallah, T. *Inorg. Chem.* **2006**, *45*, 7038–7040.

(29) Yang, E.-C.; Wernsdorfer, W.; Nakano, M.; Zakharov, L. N.; Sommer, R. D.; Rheingold, A. L.; Ledezma-Gairaud, M.; Christou, G. *J. Appl. Phys.* **2002**, *91*, 7382–7384.

(30) Zeng, M.-H.; Yao, M.-X.; Liang, H.; Zhang, W.-X.; Chen, X.-M. *Angew. Chem., Int. Ed.* **2007**, *46*, 1832–1835.

(31) Carlin, R. L. *Magnetochemistry*; Springer: Berlin, 1986.

(32) Petit, S.; Pillet, G.; Luneau, D.; Chibotaru, L. F.; Ungur, L. *Dalton Trans.* **2007**, 4582–4588.

(33) Saalfrank, R. W.; Scheurer, A.; Prakash, R.; Heinemann, F. W.; Nakajima, T.; Hampel, F.; Leppin, R.; Pilawa, B.; Rupp, H.; Muller, P. *Inorg. Chem.* **2007**, *46*, 1586–1592.

(34) Ferguson, A.; Parkin, A.; Sanchez-Benitez, J.; Kamenev, K.; Wernsdorfer, W.; Murrie, M. *Chem. Commun.* **2007**, *33*, 3473–3475.

(35) Chibotaru, L. F.; Ungur, L. The computer programs SINGLE_ANISO and POLY_ANISO. University of Leuven, 2006.

Table 1. Crystallographic Data for [Co$^{III}_4$Co$^{II}_2$(L)$_6$(MeO)$_6$]

formula	$C_{48}H_{66}Co_7F_{18}N_6O_{18}$
formula weight (g mol^{-1})	1769.6
crystal system	monoclinic
space group	$P2_1/n$ (No. 14)
a (Å)	13.409(5)
b (Å)	12.052(5)
c (Å)	20.006(5)
β (deg)	101.237(5)
V (Å^3)	3171(2)
Z	2
T (K)	293
λ(Mo Kα) (Å)	0.71069
D (g cm^{-3})	1.853
μ (mm^{-1})	1.911
θ range (deg)	2.02−20.03
R^a	0.0506
$R_w{}^b$	0.0507
S	1.22

^{a} $R = \sum|F_o - F_c|/\sum|F_o|$. ^{b} $R_w = [\sum w|F_o - F_c|^2/\sum w|F_o|^2]^{1/2}$.

Table 2. Selected Interatomic Distances (Å) in [Co$^{III}_4$Co$^{II}_2$(L)$_6$(MeO)$_6$]

Co1−O50	2.055(8)	Co1−O10	2.082(7)	Co1−O30	2.149(7)
Co2−N53	1.89(1)	Co2−O57	1.906(8)	Co2−O3	1.921(8)
Co2−O2	1.936(7)	Co2−O50	1.944(7)	Co2−O30	2.022(8)
Co3−O37	1.886(8)	Co3−O1	1.895(8)	Co3−N33	1.898(9)
Co3−O30	1.926(7)	Co3−O2	1.928(8)	Co3−O10	1.955(7)
Co4−N13	2.00(1)	Co4−O17	2.04(1)	Co4−O1	2.050(7)
Co4−O3	2.053(8)	Co4−O10	2.064(8)	Co4−O50	2.159(7)
Co1···Co3	3.066(1)	Co1···Co2	3.080(2)	Co1···Co4	3.128(2)
Co2···Co3	3.008(2)	Co3···Co4	3.106(2)		

negative magnetic anisotropies on the metal sites. The lack of SMM behavior in the investigated complex is counterintuitive, since according to eq 1, the combination of these two factors suffices to create a barrier for reversal of magnetization in complexes in the strong-exchange coupling regime.

Experimental Section

Syntheses. All of the chemicals and solvents were used as received. Ligand LH$_2$ was synthesized as previously reported.[13,25]

Preparation of [Co$^{II}_3$Co$^{III}_4$(L)$_6$(MeO)$_6$]. An excess of triethylamine (0.5 mL, 3 mmol) and 152 mg (1.2 mmol) of anhydrous CoCl$_2$ were added to 197 mg (1 mmol) of ligand LH$_2$ previously dissolved in 20 mL of MeOH. The resulting solution was stirred for few minutes, filtered to remove any solid, and set aside for slow evaporation under room conditions. After 1 week, this afforded thin, dark-brown, needle-shaped crystals suitable for single-crystal X-ray diffraction structure determination.

X-ray Crystallography. Data Collection. Diffraction data were collected at room temperature by means of the COLLECT program.[36] Lorentz-polarization correction, peak integration, and background determination were carried out with the DENZO[37] program. Frame-scaling and unit-cell parameter refinement were accomplished using the SCALEPACK program.[37] The lattice constants were refined by least-squares refinement using 3077 reflections (1.0° < θ < 20.0°). No absorption correction was applied to the data sets.

Structure Solution and Refinement. [Co$^{II}_3$Co$^{III}_4$(L)$_6$(MeO)$_6$] crystallizes in the monoclinic crystal system. According to the observed systematic extinctions, the structure was solved in the $P2_1/n$ space group (No. 14) by direct methods using the SIR97 programs[38] combined with Fourier difference syntheses and refined against F using reflections having $I/\sigma(I) > 3$ via the CRYSTALS program.[39] All of the thermal atomic displacements for non-hydrogen atoms were refined anisotropically. Crystallographic data and refinement details are summarized in Table 1. Selected interatomic distances and angles are listed in Table 2.

Magnetic Measurements. Magnetic susceptibilities were measured on polycrystalline samples in the range 2−300 K with a Quantum Design MPMS SQUID magnetometer operating at field strength of 0.5 T using a PTFE capsule as the sample holder. The magnetization was measured at 2 and 5 K in the range 0−55 kOe. The data were corrected for diamagnetism of the sample holder and of the constituent atoms using Pascal's constants.

Computational Details. The [Co$^{II}_3$Co$^{III}_4$(L)$_6$(MeO)$_6$] complex is too large to be treated as is by any explicitly correlated ab initio method. Hence, it was studied by considering separate mononuclear cobalt fragments. At this point, the main question involved how to cut the heptanuclear complex into suitable mononuclear fragments without significantly changing the energy-level structures of the magnetic centers. The cobalt ions are quite close to each other, so to have a good description within a fragment, one needs to take into account the effects of the neighboring cobalt atoms. Computationally, it is not possible to take into account the effects of the neighboring cobalt atoms completely; therefore, they were simulated using the closed-shell Li$^+$- or Zn^{2+}-embedding ab initio model potential (AIMP).[40] Keeping in mind that the molecule has inversion symmetry and moreover that the Co(III) centers are almost identical (Figure 1), we chose to consider three different fragments: the central Co(II) fragment (Co1), the marginal Co(II) fragment (Co4), and the marginal Co(III) fragment (Co2 and Co3).

The second approximation concerned the coordination sphere. In the case of single bonds with distant atoms surrounding the cobalt sites, the distant atoms were simulated by hydrogen atoms. Evidently, no geometry optimization on the fragments was done, and all of the atomic coordinates except for those of added hydrogens were taken from the crystal X-ray analysis.

The electronic structures of mononuclear cobalt fragments were calculated via the complete active space self-consistent field/complete active space second-order perturbation theory (CASSCF/CASPT2) approach using the MOLCAS 7.0 package.[41] This method is able to accurately describe the ground and excited states of various transition-metal compounds.[42] The basis sets for the metal and the atoms of the first coordination sphere were atomic natural orbitals from the MOLCAS ANO-RCC library. The contraction [6s5p3d2f1g] was used for Co and [4s3p2d1f] for nearest-neighbor O and N. More distant atoms were simulated by smaller basis sets from the ANO-S library;[43] the contraction [3s2p] was used for C, O, and F, and [2s] was used for H. The Zn^{2+} ions replacing Co^{2+} in the second coordination sphere were treated using the embedding AIMP.[44]

The choice of the CASSCF active space included the Co 3d orbitals, since we were interested in ligand-field states, an additional d shell taking into account the 3d double-shell effect,[45] and one doubly occupied ligand orbital for the marginal Co(III) sites. The inclusion of the doubly occupied ligand orbital into the active space usually improves the CASSCF wave function. The remaining

---

(36) COLLECT; Nonius B. V.: Delft, The Netherlands, 1997−2001.

(37) Otwinowski, Z.; Minor, W. *Methods Enzymol.* **1997**, *276*, 307–326.

(38) Cascarano, G.; Altomare, A.; Giacovazzo, C.; Guagliardi, A.; Moliterni, A. G. G.; Siliqi, D.; Burla, M. C.; Polidori, G.; Camalli, M. *Acta Crystallogr.* **1996**, *A52*, C-79.

(39) Watkin, D. J.; Prout, C. K.; Carruthers, J. R.; Betteridge, P. W. CRYSTALS, Issue 11; Chemical Crystallography Laboratory: Oxford, U.K., 1999.

(40) Seijo, L.; Barandiaran, Z. *Comput. Chem. (Singapore)* **1999**, *4*, 55–152.

(41) Karlström, G.; Lindh, R.; Malmqvist, P.-Å.; Roos, B. O.; Ryde, U.; Veryazov, V.; Widmark, P.-O.; Cossi, M.; Schimmelpfennig, B.; Neogrady, P.; Seijo, L. *Comput. Mater. Sci.* **2003**, *28*, 222–239.

(42) Pierloot, K. *Mol. Phys.* **2003**, *101*, 2083–2094.

(43) Pierloot, K.; Dumez, B.; Widmark, P.-O.; Roos, B. O. *Theor. Chim. Acta* **1995**, *90*, 87–114.

(44) López-Moraza, S.; Pascual, J. L.; Barandiarán, Z. *J. Chem. Phys.* **1995**, *103*, 2117–2125.

(45) Andersson, K.; Roos, B. O. *Chem. Phys. Lett.* **1992**, *191*, 507–514.

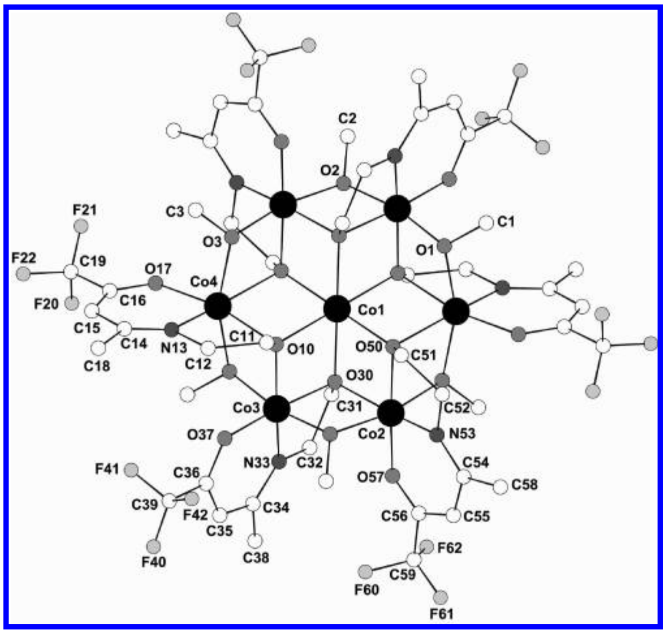

Figure 1. Molecular structure of $[Co^{II}_3Co^{III}_4L_6(MeO)_6]$ with atom labels included. The hydrogen atoms have been omitted for clarity.

dynamical correlation effects were treated in the subsequent CASPT2 step. All of the valence electrons (3p and 3d in Co, 2s and 2p in C, N, O, and F, and 1s in H) were correlated. An imaginary level shift of 0.1 eV was used in all of the CASPT2 calculations in order to avoid problems with intruder states.[46] The effect of spin−orbit coupling on the lowest states was taken into account within the RASSI program of MOLCAS.[41] In this procedure, the matrix elements of the spin−orbit interaction are calculated within the CASSCF wave function while the CASPT2 energy corrections of the corresponding states are added on the diagonal of the spin−orbit matrix. Such an approach also proved to be efficient for strongly covalent complexes.[47]

With the spin−orbit multiplets obtained in this way, the powder susceptibility and the **g** tensors for the lowest Kramers doublets of the isolated fragments were further evaluated using the recently developed ab initio methodology, which is now available as a FORTRAN routine interfaced with MOLCAS.[35]

Exchange interactions between metal sites were taken into account within the Lines model.[48] This approach begins with the isotropic exchange interactions that would exist in the absence of spin−orbit coupling on the metal sites. It has been already used successfully to describe the Ln radical exchange interaction.[49] The corresponding isotropic exchange parameters are the only fitting parameters of the theory. Diagonalizing the matrix of the corresponding Heisenberg Hamiltonian, written in the basis of spin−orbit multiplets of cobalt fragments obtained from our quantum-chemistry calculations, gave solutions corresponding to anisotropic exchange interactions between the sites. The solutions obtained for the spin−orbit states were then used for the calculation of magnetic properties of the polynuclear complex via a specially designed FORTRAN routine.[35] This approach has recently been successfully applied for the treatment of magnetism in Co(II) complexes[32] and Dy(III) triangles.[50]

Results and Discussion

Description of the Crystal Structure. The asymmetric unit comprises four crystallographically independent cobalt ions (Co1, Co2, Co3, and Co4) with three independent L^{2-} ligands and three independent methoxy groups. Co1 is located on an inversion center, and the other cobalt ions are in general positions. Because of the symmetries of the space group ($P2_1/n$), this affords neutral, centrosymmetric, wheel-shaped heptanuclear clusters having the general formula $[Co_7(L)_6(MeO)_6]$ (Figure 1). Co1 occupies the center of the wheel, while Co2, Co3, Co4, and their centrosymmetric equivalents are on the rim. Each of the seven cobalt ions is in a pseudo-octahedral coordination environment. However, the environment of the central cobalt differs from those of the others. Indeed, the coordination sphere of the central cobalt ion (Co1) consists only of oxygen atoms, each of which comes from the 2-aminoethanol moiety of one of the six peripheral ligands and connects the central cobalt ion with two of the peripheral cobalt ions in a μ_3-alkoxo fashion. The six other cobalt ions exhibit identical NO_5 environments, in which two oxygen atoms and one nitrogen atom belong to one of the L^{2-} ligands, a third oxygen atom (μ_3-alkoxo) comes from another L^{2-} ligand, and the last two oxygen atoms come from two μ_2-bridging methoxy groups. Each methoxy group bridges two peripheral cobalt ions.

As the cluster is neutral, it follows from the charge balance that three cobalt ions should be in the 2+ valence state and four in the 3+ valence state, leading to the formula $[Co^{II}_3Co^{III}_4(L)_6(MeO)_6]$. An analysis of the Co−O and Co−N bond lengths (Table 2), which are longer for Co1 and Co4 (which average 2.082 and 2.00 Å, respectively) than for Co2 and Co3 (which average 1.932 and 1.894 Å, respectively) indicates that Co1 and Co4 are in a lower oxidation state than Co2 and Co3. Thus, the 2+ valence state is attributed to Co1 and Co4 and the 3+ valence state to Co2 and Co3. In order to confirm these valence-state attributions, bond valence sum (BVS) calculations[51−53] were performed for each cobalt center; indeed, the BVS calculations for Co1 and Co4 (Co1 = 2.02 and Co4 = 2.38) agreed with the 2+ valence state, whereas those for Co2 and Co3 (Co2 = 3.47 and Co3 = 3.48) indicated a 3+ valence state. All of the bond lengths (C−O, C−N, and C−F) within the L^{2-} ligands and the methoxy groups were in agreement with our previous findings for tetranuclear and nonanuclear complexes.[13,25] Such a wheel-shaped structure has been observed in several other heptanuclear complexes.[54−57] Most of them are mixed-valent $[M^{II}_3M^{III}_4]$,[54−56] and one concerns a $[Co^{II}_4Co^{III}_3]$ fragment in a coordination polymer.[54]

Magnetic Properties. At 300 K, the product of the magnetic susceptibility and temperature (χT) was 10.61 cm^3 K mol^{-1}

---

(46) Forsberg, N.; Malmqvist, P.-Å. *Chem. Phys. Lett.* **1997**, *274*, 196–204.

(47) (a) Hendrickx, M. F. A.; Mironov, V. S.; Chibotaru, L. F.; Ceulemans, A. *J. Am. Chem. Soc.* **2003**, *125*, 3694–3695. (b) Hendrickx, M. F. A.; Mironov, V. S.; Chibotaru, L. F.; Ceulemans, A. *Inorg. Chem.* **2004**, *43*, 3142–3150.

(48) Lines, M. E. *J. Chem. Phys.* **1971**, *55*, 2977–2984.

(49) Kahn, M. L.; Ballou, R.; Porcher, P.; Kahn, O.; Sutter, J. P. *Chem.—Eur. J.* **2002**, *8*, 525–531.

(50) Chibotaru, L. F.; Ungur, L.; Soncini, A. *Angew. Chem., Int. Ed.* **2008**, *47*, 4126–4129.

(51) Brese, N. E.; O'Keeffe, M. *Acta Crystallogr.* **1991**, *B47*, 192–197.

(52) Brown, I. D.; Altermatt, D. *Acta Crystallogr.* **1985**, *B41*, 244–247.

(53) Thorp, H. H. *Inorg. Chem.* **1992**, *31*, 1585–1588.

(54) Alley, K. G.; Bircher, R.; Waldmann, O.; Ochsenbein, S. T.; Güdel, H. U.; Moubaraki, B.; Murray, K. S.; Fernandez-Alonso, F.; Abrahams, B. F.; Boskovic, C. *Inorg. Chem.* **2006**, *45*, 8950–8957.

(55) Koizumi, S.; Nihei, M.; Shiga, T.; Nakano, M.; Nojiri, H.; Bircher, R.; Waldmann, O.; Ochsenbein, S. T.; Güdel, H. U.; Fernandez-Alonso, F.; Oshio, H. *Chem.—Eur. J.* **2007**, *13*, 8445–8453.

(56) Oshio, H.; Hoshino, N.; Ito, T.; Nakano, M.; Renz, F.; Gutlich, P. *Angew. Chem., Int. Ed.* **2003**, *42*, 223–225.

(57) Tesmer, M.; Müller, B.; Vahrenkamp, H. *Chem. Commun.* **1997**, 721–722.

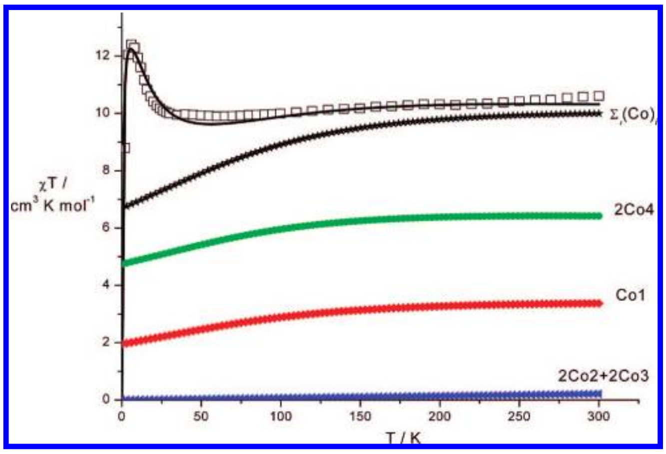

Figure 2. Experimental temperature dependence of χT measured on powders (☐) compared with calculated contributions from individual Co(III) fragments (blue triangles), Co(II) fragments (red diamonds and green circles), and their sum (black stars); the solid line shows the result of including the effects of exchange interactions with parameter values $J_1 = 1.5$ cm^{-1}, $J_2 = 5.5$ cm^{-1}, and $zJ' = -0.03$ cm^{-1}. The ab initio calculations were done within structural model C for the cobalt sites (see the text for details).

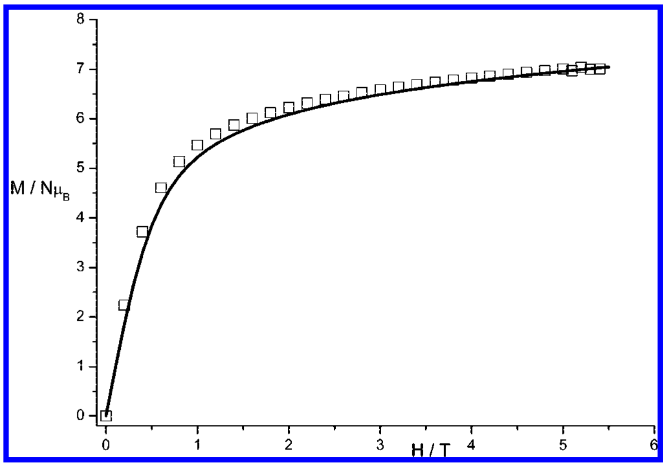

Figure 3. Molar magnetization of $[Co^{II}_3Co^{III}_4(L)_6(MeO)_6]$ measured at 2 K (☐) and calculated within structural model C using the exchange parameter values $J_1 = 1.5$ cm^{-1}, $J_2 = 5.5$ cm^{-1}, and $zJ' = -0.03$ cm^{-1} (solid line).

(Figure 2). As the temperature was decreased, χT decreased slightly to reach a minimum at 60 K (9.90 cm^3 K mol^{-1}), then increased to the maximum value of 12.40 cm^3 K mol^{-1} at 6 K, and then decreased continuously at lower temperatures.

The χT value obtained at room temperature (10.61 cm^3 K mol^{-1}) seems to support a high spin ($S = {}^3/_2$) on Co(II) and a low spin ($S = 0$) on Co(III), since the assumption of $S = 2$ for the latter would result in much larger values. However, the field dependence of the magnetization at 2 K cannot be easily reconciled with the ferromagnetic susceptibility in Figure 2. Indeed, Figure 3 shows a magnetization of 6.8μ_B at 4 T ($\mu_B H/k_B T = 2$), which could be reproduced for $g = 2$ and a total spin $S = {}^7/_2$,[58] while both of these quantities were expected to be larger. It follows from these estimates that the magnetic anisotropy on the cobalt centers plays an important role. Therefore, we considered this problem by performing ab initio calculations on mononuclear cobalt fragments of this complex, as discussed in the following section.

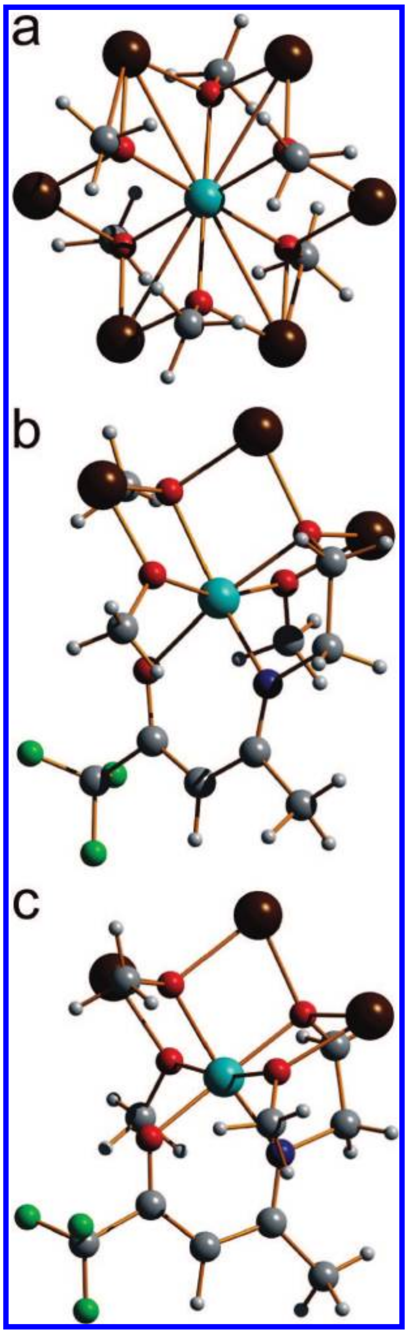

Figure 4. Structural model C used in the ab initio calculations on the mononuclear fragments: (a) the central Co(II) site; (b) the marginal Co(II) site; (c) the Co(III) site. Color scheme: turquoise, Co; red, O; green, F; blue, N; brown, Zn^{2+}; gray, C; white, H.

Ab Initio Calculations on Mononuclear Cobalt Fragments. In order to gain insight into the magnetic properties of the Co_7 wheel, we first investigated the lowest molecular terms and spin−orbit multiplets of mononuclear cobalt fragments by a series of ab initio calculations.

We chose three structural models of the fragment. In models A and B (see Figures 1S and 2S, respectively, in the Supporting Information), the cobalt ions nearest a given fragment were replaced by Li^+ ions, while in model C (Figure 4), they were replaced by the Zn^{2+} AIMP. In the case of the central cobalt site, the second coordination sphere was modeled by hydrogens in A, while the CH_3 fragments were kept in B and C (Figure 4a). The same applies for the marginal Co(II) and Co(III) sites, where the distant CF_3 and CH_3 groups bound to the conjugated

---

[58] Kahn, O. *Molecular Magnetism*; VCH Publishers: New York, 1993.

Table 3. CASSCF/CASPT2 Energies of the Lowest Terms of the Central Co(II) Fragment in Different Structural Approximations

spin mult.	CASSCF energy (cm^{-1})			CASPT2 energy (cm^{-1})			octahedral parent term
	A	B	C	A	B	C	
4	0.0	0.0	0.0	0.0	0.0	0.0	$^4T_{1g}$
4	224.2	285.0	379.6	251.1	474.2	224.2	
4	344.8	520.0	672.7	423.4	902.9	602.2	
4	5929.0	6297.2	7104.9	6520.7	6919.1	7935.7	$^4T_{2g}$
4	6810.3	7199.2	8014.7	7143.4	7612.9	8552.7	
4	7051.8	7637.4	8126.7	7467.1	8107.5	8749.6	
4	13944.2	14757.9	16111.5	15395.5	16370.2	17875.9	$^4A_{2g}$
2	13782.8	13414.0	11604.6	11866.7	11268.4	9877.2	^2E_g
2	15350.3	15076.8	13368.4	13359.4	12872.6	11660.0	
2	19401.3	19310.5	18403.5	16735.6	16472.8	16339.5	$^2T_{1g}$
2	19569.5	19645.9	18463.3	17070.4	17074.6	16478.4	
2	19621.5	19700.2	18506.2	17516.8	17379.6	16859.5	

Table 4. Energies (cm^{-1}) of the Kramers Doublets Arising from Low-Lying Quartets of Octahedral $^4T_{1g}$ (First Six Lines) and $^4T_{2g}$ (Last Six Lines) Parentage on the Central Co(II) Fragment, Calculated in Three Structural Approximations

A	B	C
0.0	0.0	0.00
249.4	180.6	231.08
455.7	619.4	486.34
846.0	898.0	821.70
992.8	1263.8	1108.10
1088.5	1376.7	1176.86
6918.0	7202.2	8302.70
6980.0	7265.2	8358.99
7545.4	7893.8	8906.29
7571.5	7921.9	8929.86
7876.2	8394.6	9132.92
7969.8	8483.9	9243.83

Table 5. CASSCF/CASPT2 Energies of the Lowest Terms of the Marginal Co(II) Fragment in Different Structural Approximations

spin mult.	CASSCF energy (cm^{-1})			CASPT2 energy (cm^{-1})			octahedral parent term
	A	B	C	A	B	C	
4	0.0	0.0	0.0	0.0	0.0	0.0	$^4T_{1g}$
4	260.3	348.8	111.6	222.8	331.0	84.3	
4	1505.2	1616.6	1532.9	1634.2	1797.6	1602.1	
4	7327.3	7742.8	7264.4	8312.6	8904.5	8087.0	$^4T_{2g}$
4	8434.0	8698.5	8549.9	9148.5	9558.4	9269.0	
4	8745.8	9129.6	8884.1	9356.4	9878.4	9509.3	
4	16756.4	17312.7	16921.2	18367.6	18989.2	18475.6	$^4A_{2g}$
2	13421.5	13119.2	13215.4	11126.7	10377.8	11053.2	^2E_g
2	13717.9	13637.1	13359.2	11393.0	10964.2	11135.6	
2	19524.2	19503.5	19332.6	16745.5	16681.3	17613.1	$^2T_{1g}$
2	19628.7	19661.3	19476.7	16982.0	16882.1	17658.2	
2	20035.1	20158.6	19874.6	17012.2	17036.4	17799.7	

ring were also taken into account in C (Figures 4b,c, respectively). In the latter case, the two Co(III) fragments Co2 and Co3 (Figure 1) are structurally different, since they are not related by symmetry; this results in tiny differences in their geometries (bond lengths and angles). The consideration of several structural models for the fragments allowed us to assess the errors in the calculated molecular terms and spin−orbit multiplets introduced by fragmentation and to check the robustness of our final results.

Central Co(II) Fragment (Co1). The results of the CASSCF/CASPT2 calculations on the central cobalt fragment are presented in Table 3. The central Co(II) ion was found to lie in a slightly elongated octahedral environment (Table 2) that is compressed along the axis perpendicular to the Co_7 plane, which lifts the degeneracy of the 3d orbitals completely. Besides geometrical distortion of the oxygen octahedron, there is a distortion of electronic density around each oxygen ion, since it is surrounded by two other cobalt ions and one CH_3 group (Figure 4a). This leads to additional low-symmetry components of the ligand field.[32] Nevertheless, splitting of the orbital components of the terms is not strong, allowing the recognition of the parent ground $^4T_{1g}$ and first excited $^4T_{2g}$ orbital triplets (see Table 3).

The lowest three quartet-spin states emerging from the ground orbital triplet $^4T_{1g}$ were found to be quite close in energy, indicating a weak effect of the low-symmetry ligand field. Table 3 shows that the energy intervals between three lowest quartets are roughly equal, which is probably the result of competition between two axial ligand fields, one arising from the compression of the oxygen octahedron along the axis perpendicular to the Co_7 plane and the other being determined by the elongation of the Co_1-O_{30} bonds (Figure 1). The mixing of these quartets by the spin−orbit interaction is supposed to be considerable because the magnitude of the spin−orbit interaction is on the same order as their energy separation.

The effects of the spin−orbit interaction were evaluated by mixing all 10 ligand-field quartet states and 40 doublet states. The energies of several low-lying Kramers doublets are shown in Table 4. Despite some differences in the energies obtained for the lowest Kramers doublets within the different structural approximations, they all show strong mixing between the three low-lying quartet states by spin−orbit coupling.

The spread of the energies of the six lowest Kramers doublets is at least twice as large as the energy separations between three quartet states in Table 3. Consequently, we could not assign the Kramers doublets in Table 4 to some parent quartets, which means that they cannot be understood as a zero-field splitting (ZFS) of a given $S = {}^3/_2$ level. A similar situation has recently been found in other pseudo-octahedral Co(II) complexes.[59,60]

Marginal Co(II) Fragment (Co4). The carbon atoms entering the NCCCO chain in this fragment (Figure 4b) cannot be modeled by hydrogen in a lower approximation because of the presence of π conjugation in the chain, which should affect the ligand-field terms. Therefore, this chain was retained in structural model A (see Figure 1S in the Supporting Information). The results of the CASSCF/CASPT2 calculations on the three structural models are shown in Table 5.

The marginal Co(II) ion lies in a quite different pseudo-octahedral environment than the central Co(II). Beside variations in the Co−O bond lengths and deviations of the O−Co−O angles from 90°, important deviations from an octahedral crystal field are caused by the presence of one nitrogen atom replacing one oxygen in the pseudo-octahedral oxygen environment. As Table 5 shows, the ground $^4T_{1g}$ term splits into two spin quartets that are close in energy and one that is well-separated from them. The overall splitting of these quartets is much larger than in the case of the central cobalt fragment, which is due to a stronger departure from an octahedral ligand field. The energy difference between the two lowest quartets does not vary much in the different structural models and is comparable with the spin−orbit interaction for a Co(II) ion. Therefore, we again expected strong mixing of the terms by spin−orbit coupling.

The effects of the spin−orbit interaction were evaluated as in the previous case, and the energies of the low-lying Kramers

---

(59) Clima, S.; Hendrickx, M. F. A.; Chibotaru, L. F.; Soncini, A.; Mironov, V.; Ceulemans, A. *Inorg. Chem.* **2007**, *46*, 2682–2690.

(60) Herrera, J. M.; Bleuzen, A.; Dromzee, Y.; Julve, M.; Lloret, F.; Verdaguer, M. *Inorg. Chem.* **2003**, *42*, 7052–7059.

Table 6. Energies (cm^{-1}) of the Kramers Doublets Arising from Low-Lying Quartets of Octahedral $^4T_{1g}$ (First Six Lines) and $^4T_{2g}$ (Last Six Lines) Parentage on the Marginal Co(II) Fragment, Calculated in Three Structural Approximations

A	B	C
0.0	0.0	0.00
199.4	185.8	243.72
504.7	574.6	483.94
754.5	791.6	765.01
1964.1	2086.8	2017.61
2014.9	2140.5	2060.73
8594.9	9153.4	8460.46
8662.3	9206.1	8516.02
9432.0	9817.8	9642.50
9466.9	9842.5	9666.82
9659.7	10142.0	9893.43
9756.2	10228.2	9981.98

doublets are shown in Table 6. The resulting splitting of the four lowest Kramers doublets is much larger than the energy separation between the lowest quartets in Table 5. Therefore, as in the previous case, the ZFS is ill-defined for this fragment.

Marginal Co(III) Fragments (Co2, Co3). At first glance, the structure of these fragments (Figure 4c) looks similar to that of the marginal Co(II) sites (Figure 4b). However, as mentioned in Description of the Crystal Structure, they differ in the Co−O and Co−N bond lengths, which are longer in the latter structure (Table 2). The octahedral Co(III) complexes were found to have a quintet $^5T_{2g}$ ground term for a weak ligand field and a singlet $^1A_{1g}$ ground term for a strong ligand field. The ligand-field parameter 10Dq is 20000−24000 cm^{-1} when the ligands are amines, 2,2′-bipyridyl, and ammonia, while it is ∼19000 cm^{-1} for water and 18600 cm^{-1} for hydroxide ion.[61] In our case, the ligand field created by five oxygens and one nitrogen is expected to be ∼20000 cm^{-1}. According to Tanabe−Sugano diagrams,[61,62] such a strength of 10Dq places the ground state close to the intersection of the quintet and singlet terms. Therefore, a trustworthy estimate of the relative energies of the lowest states could only be obtained from ab initio calculations.

The results of the CASSCF/CASPT2 calculations on the different model fragments are shown in Table 7. They show that the ground state for the Co(III) sites is a spin singlet for all three models of the fragment. The first excited spin quintet lies at least 700 cm^{-1} higher for all of the structural models. As a result, the ground state remained nonmagnetic even when the spin−orbit coupling was included. The results of the spin−orbit coupling calculations are shown in Table S1 in the Supporting Information. All of the spin−orbit states were found to be nondegenerate, in agreement with the low symmetry of the fragments [Co(III) is not a Kramers ion]. The results show that the ground state is well-separated from the first excited states.

Table 7. CASSCF/CASPT2 Energies of the Lowest Terms of Different Spin Multiplicity of the Marginal Co(III) Fragments in Different Structural Approximations

spin mult.	A		B		C		octahedral parent term
	Co2	Co3	Co2	Co3	Co2	Co3	
				CASSCF Energy (cm^{-1})			
1	2816.4	1447.3	2031.4	682.5	0.0	0.0	$^1A_{1g}$
1	15773.1	15221.5	15710.9	15060.8	13054.3	13791.0	$^1T_{1g}$
1	18192.4	17163.8	16931.9	16142.2	16408.9	17244.5	
1	19445.6	18899.4	19322.8	18680.7	19436.2	18856.6	
3	5187.3	4599.3	5220.5	4876.5	3586.0	4395.1	$^3T_{1g}$
3	8338.9	7601.3	6546.1	5764.4	5741.2	6804.8	
3	8769.0	8771.6	8895.4	7997.9	8408.8	9591.0	
5	0.0	0.0	0.0	0.0	2049.4	2842.2	$^5T_{2g}$
5	1745.0	1632.7	2072.4	2001.3	3416.2	4176.5	
5	2575.5	2419.4	2928.4	2822.6	4501.7	5018.4	
				CASPT2 Energy (cm^{-1})			
1	0.0	0.0	0.0	0.0	0.0	0.0	$^1A_{1g}$
1	12667.4	13385.0	13156.2	13722.5	14017.2	14713.4	$^1T_{1g}$
1	14955.2	15590.2	14790.1	15203.9	16067.2	17186.7	
1	15246.0	16080.2	15775.7	16615.2	16283.7	17596.3	
3	1721.8	2469.7	2129.9	3085.8	1565.7	2740.8	$^3T_{1g}$
3	3827.8	5423.5	3747.1	4696.9	2534.5	4445.2	
3	4645.5	5718.5	4068.3	5250.3	5874.4	7655.7	
5	736.8	2171.2	1779.9	3049.8	4081.1	5527.4	$^5T_{2g}$
5	2863.2	4189.3	4461.0	5670.8	5973.9	7451.2	
5	4143.3	5274.1	5903.9	6968.8	7485.6	8390.5	

Table 8. Contributions to χT (cm^3 K mol^{-1}) at 300 K from Individual Cobalt Sites, Calculated within Different Structural Approximations

	A	B	C
central Co(II)	3.42	3.21	3.37
2 × marginal Co(II)	6.22	6.09	6.42
2 × Co2-type marginal Co(III)	0.51	0.18	0.13
2 × Co3-type marginal Co(III)	0.14	0.13	0.09
total	10.29	9.61	10.01

Magnetic Properties of Individual Cobalt Sites. The ab initio results obtained above were used for calculations of the magnetic properties of the individual cobalt fragments using the routine SINGLE-ANISO.[35] Table 8 and Figure 2 present the contributions of the individual cobalt fragments to the overall magnetic susceptibility. We can see that at room temperature, the sum of contributions from individual cobalt fragments already compares well with experimental value of χT for the complex. The strongest contribution comes from the central Co(II) fragment, which is not surprising in view of the small energy separation between lowest three quartets for this fragment (Table 4). The obtained values vary with the structural model used, but the deviations are much smaller for magnetic Co(II) than for nonmagnetic Co(III) sites.

The paramagnetically inactive Co(III) ions show a significant temperature-independent paramagnetic (TIP) contribution to the total susceptibility ($\chi_{\mathrm{TIP}} = 8.5 \times 10^{-4}$ cm^3 mol^{-1} and $\chi T =$ 0.25 cm^3 K mol^{-1} for one Co2 fragment in model A). As shown in Table 8, neglect of these contributions results in sensitive errors. The reason for the large TIP contribution from the Co(III) sites is that the excitation energies to reach paramagnetic states are small, as can be seen in Table 7 and Table 1S in the Supporting Information.

The much-smaller excitation energies of the lowest states explain the significant TIP contribution from the Co2 sites obtained within structural model A. These excited states arise from the first excited spin quintet (see Table 7), whose energy is only 737 cm^{-1} for model A. Recently it was shown that the CASSCF/CASPT2 method gives relatively large errors for excitation energies to terms whose spins differ much from the ground-state spin (e.g., for singlet−quintet transitions) if the conventional basis is employed.[63] This explains why we obtained much larger relative variations for calculated TIP contributions within the different structural models than for paramagnetic contributions to susceptibility.[64]

---

(61) Figgis, B. N.; Hitchman, M. A. *Ligand Field Theory and Its Applications*; Wiley: New York, 1999.

(62) Tanabe, Y.; Sugano, S. *J. Phys. Soc. Jpn.* **1954**, *9*, 753–766.

(63) Pierloot, K.; Vancoillie, S. *J. Chem. Phys.* **2006**, *125*, 124303.

Table 9. Main Values of the **g** Tensors in the Ground Kramers Doublets of Cobalt(II) Fragments, Calculated ab Initio within Three Structural Approximations

	central Co(II)			marginal Co(II)		
	g_1	g_2	g_3	g_1	g_2	g_3
A	2.778	4.311	5.899	1.382	1.668	8.240
B	2.153	4.052	6.337	1.409	1.807	8.059
C	2.506	4.000	6.324	1.464	1.596	8.429

In order to assess the magnetic anisotropy in the ground Kramers doublets of the fragments, we performed ab initio calculations of the **g** tensors using the described methodology.[35] The results are shown in Table 9.

We can see that in all of the structural approximations employed, the marginal Co(II) sites show strong axial anisotropy. This is the result of quasi-axial splitting of the $^4T_{1g}$ term (Table 5), which leads to a quasi-axial **g** tensor as well.[65] The main values obtained for the corresponding **g** tensor are reminiscent of a negative ZFS of an $S = {}^3/_2$ state strongly enhanced by orbital contributions, i.e., corresponding to a ground Kramers doublet of the $M_S = \pm{}^3/_2$ type.[66] Contrarily, the main values of the **g** tensor for the central Co(II) ion are reminiscent of a Kramers doublet of the $M_S = \pm{}^1/_2$ type arising from ZFS of an $S = {}^3/_2$ state. The relative orientations of the magnetic axes on the various Co(II) sites are shown in Figure 5.

The main magnetic axis on the marginal Co(II) sites, corresponding to g_3 in Table 9, gives the orientation of the quasi-axial ligand-field component. As we can see in Figure 5, this axis is directed along one short Co−O bond. For the central Co(II), the main magnetic axis, corresponding to g_1 in Table 9, is directed along the longest bond, Co1−O30 (Figure 1).

Effect of Exchange Interactions on the Magnetism of the $[Co^{II}_3Co^{III}_4(L)_6(MeO)_6]$ Complex. The exchange interactions among the three Co(II) ions in the complex have been taken into account within the Lines model,[48] which ascribes to each pair of magnetic ions an isotropic Heisenberg exchange interaction that would exist in the absence of spin−orbit interactions on the metal sites. As was already mentioned (see Computational Details), when the matrix of this interaction is diagonalized within the basis of several Kramers doublets on the cobalt sites obtained in the ab initio calculations, the resulting exchange states correspond to anisotropic exchange interactions between the sites. The advantage of this approach is that it allows the main contributions to the anisotropic exchange interaction to be simulated using a single parameter (J) of the ascribed isotropic exchange interaction instead of introducing nine exchange parameters for each pair of metal ions. This was especially convenient in our case, where the lack of symmetry of exchange-coupled pairs does not allow us to choose the relevant contributions to the anisotropic exchange, which would force us to consider all nine parameters. The calculations of spin−orbit exchange states and magnetic properties of the whole exchange-coupled complex were done with the routine POLY-ANISO.[35]

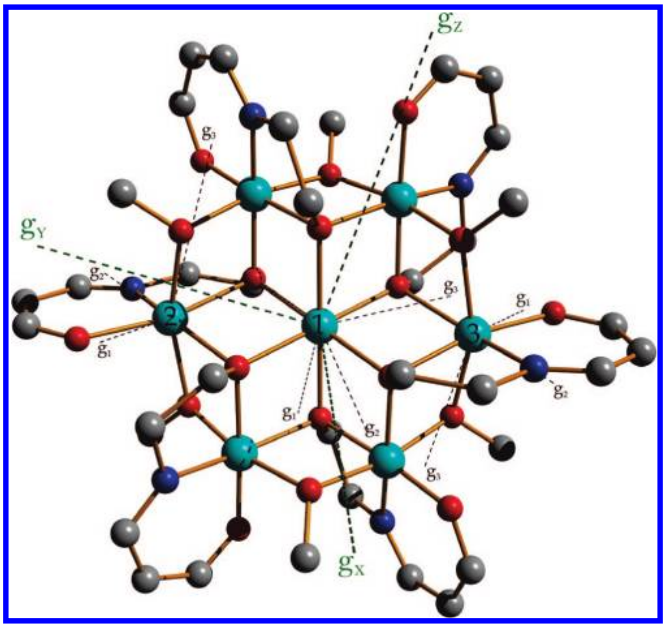

Figure 5. Orientations of the local magnetic axes on the Co(II) sites and of the magnetic axes for the whole $[Co^{II}_3Co^{III}_4(L)_6(MeO)_6]$ complex, calculated within structural model C. The numbers within the balls correspond to the numbering of the Co(II) ions used in eq 2.

In the case of $[Co^{II}_3Co^{III}_4(L)_6(MeO)_6]$, because of the inversion symmetry of the complex (Figure 5), only two isotropic exchange parameters were required. Thus, the Heisenberg Hamiltonian of the Lines model has the form

$$\hat{H}_{ex} = -J_1(\hat{\mathbf{S}}_1 \cdot \hat{\mathbf{S}}_2 + \hat{\mathbf{S}}_1 \cdot \hat{\mathbf{S}}_3) - J_2\hat{\mathbf{S}}_2 \cdot \hat{\mathbf{S}}_3 \qquad (2)$$

where $S_1 = S_2 = S_3 = {}^3/_2$. The calculated powder magnetic susceptibility (multiplied by T) as a function of temperature and powder magnetization as function of field, both for structural model C, are shown in Figures 2 and 3. The calculated magnetic properties are not strongly dependent on the structural approximation used in the ab initio fragment calculations. Figure 6 shows $\chi(T)T$ and $M(H)$ calculated using ab initio results obtained for model A. Comparison with Figures 2 and 3 shows that the two structural models give very similar results for the calculated magnetic properties (see Figure 3S in the Supporting Information for the corresponding calculated results for model B).

A small intermolecular exchange interaction described by the parameter zJ' (where z is the number of nearest-neighbor molecules)[58] was also taken into account; J_1, J_2, and zJ' were the only fitting parameters employed in our treatment. It should be noted that the contributions of Co(III) to the magnetization were also taken into account, despite the fact that they are not active in the exchange interaction. Comparison of Figures 2 and 6 shows that the main difference between structural models A and C is the slightly different predicted slope of χT with temperature near room temperature. This is the result of different accounts of the TIP contributions arising from the Co(III) sites within the two models, as discussed above.

Figure 2 shows that the exchange interaction between cobalt sites is overall ferromagnetic. We tried several sets of ferromagnetic exchange parameters: (i) nearest-neighbor interactions much stronger than the next-nearest-neighbor ones, (ii) com-

---

(64) It was shown in ref 63 that a significant improvement in the calculated singlet−quintet excitation energies can be achieved by enlarging the basis set on the metal and nearest-neighbor atoms. This would improve the calculated TIP contributions of the individual fragments as well. However, the corresponding calculations were too costly to be justified for the present problem.

(65) Chibotaru, L. F.; Hendrickx, M. F. A.; Clima, S.; Larionova, J.; Ceulemans, A. *J. Phys. Chem. A* **2005**, *109*, 7251–7257.

(66) For the Kramers doublets arising from axial ZFS of an $S = {}^3/_2$ state with $g = 2$, we have the following main values of the corresponding **g** tensors: $g_x = g_y = 0$ and $g_z = 6$ for the Kramers doublet of the $M_S = \pm{}^3/_2$ type and $g_x = g_y = 4$ and $g_z = 2$ for the Kramers doublet of the $M_S = \pm{}^1/_2$ type.

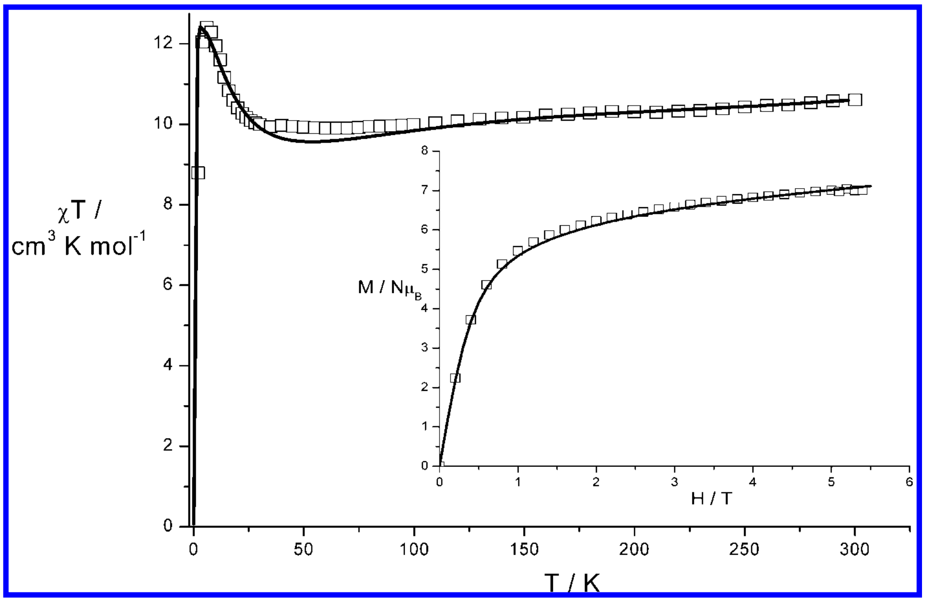

Figure 6. Experimental temperature dependence of χT measured on powders (☐) compared with the ab initio calculated magnetic susceptibility ($J_1 = 1.4$ cm^{-1}, $J_2 = 5.6$ cm^{-1}, $zJ' = -0.01$ cm^{-1}) within structural model A for the cobalt sites (solid line). Inset: the measured molar magnetization at 2 K (☐) compared with the ab initio calculated results for structural model A with the same exchange parameter values (solid line).

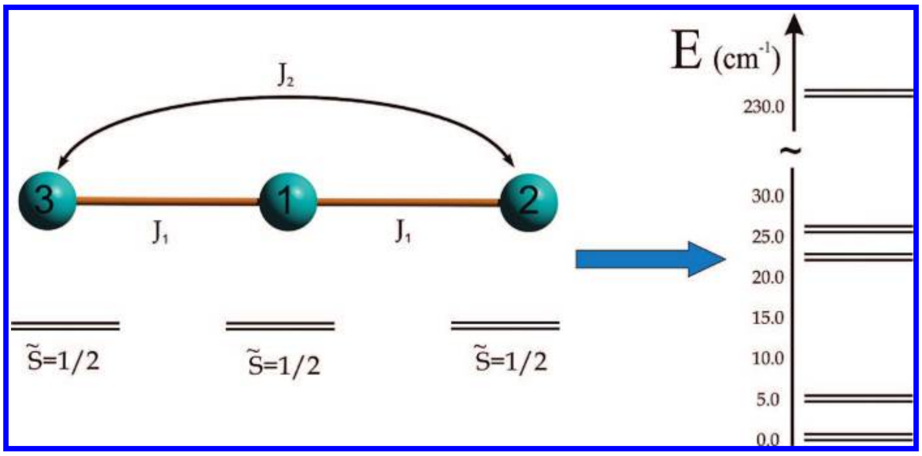

Figure 7. The spectrum of the lowest spin−orbit exchange states of the $[Co^{II}_3Co^{III}_4(L)_6(MeO)_6]$ complex calculated using the exchange parameter values $J_1 = 1.5$ cm^{-1}, $J_2 = 5.5$ cm^{-1}, and $zJ' = -0.03$ cm^{-1}.

parable interactions among all three cobalt sites, and (iii) nearest-neighbor interactions much weaker than the next-nearest-neighbor ones. A comparison of the simulated magnetic properties with experiment shows that the last set is the best. The calculations shown in Figures 2 and 3 were performed using the values $J_1 = 1.5$ cm^{-1}, $J_2 = 5.5$ cm^{-1}, and $zJ' = -0.03$ cm^{-1}. We note that the relatively strong next-nearest-neighbor ferromagnetic exchange interaction is not unrealistic when the centers are connected via diamagnetic metal ions with low electron-promotion energies between neighboring metals. Thus, in the recently investigated thiophenolate-bridged complex $[LFe^{III}Co^{III}Fe^{III}L]^{3+}$ having a relatively low electron-promotion energy between cobalt and iron sites, the exchange interaction between distant ferric sites was found to be $J_{Fe-Fe} = 42$ cm^{-1}.[67] Another well-known example is the Prussian blue molecular magnet, in which the interaction between next-nearest-neighbor high-spin Fe(III) sites is mediated by a bridge containing the diamagnetic Fe(II) ion. Here again, the low electron-promotion energy between the Fe(II) and Fe(III) sites seems to be the reason for the relatively strong ferromagnetic interaction between distant magnetic ions. In the present case, there are two Co(II)−Co(III)−Co(III)−Co(II) exchange pathways with a priori low electron-promotion energies between heterovalent metal sites, which favor the relatively strong exchange interaction between distant Co(II) sites.

The lowest spin states of the complex are very anisotropic and cannot be seen as arising from the splitting of the lowest free spin-exchange levels by anisotropic terms, as is the case, for instance, in molecular clusters of $Mn_{12}O_{12}$ acetate.[1,2] Indeed, given the much larger separation of the lowest Kramers doublets on Co(II) sites in comparison with J_1 and J_2, the lowest spin−orbit multiplets of the cluster arise from the exchange interaction between the lowest Kramers doublets on each Co(II) site. Figure 7 shows that the lowest Kramers doublets of the cluster (the four lowest levels on the right-hand side of Figure 7) all lie within an energy interval of ~30 cm^{-1} and are separated from the next ones, involving excited Kramers doublets on cobalt sites, by ~180 cm^{-1}. This is the main feature distinguishing the present complex from the class of polynuclear

---

(67) Chibotaru, L. F.; Girerd, J.-J.; Blondin, G.; Glaser, T.; Wieghardt, K. *J. Am. Chem. Soc.* **2003**, *125*, 12615–12630.

Table 10. Main Values of the **g** Tensor of the Ground Kramers Doublet of the $[\mathrm{Co^{II}_3Co^{III}_4(L)_6(MeO)_6}]$ Complex Calculated in Three Structural Approximations

	g_X	g_Y	g_Z
A	0.277	0.360	19.787
B	0.377	0.617	18.650
C	0.086	0.133	20.276

exchange compounds with relatively weak ZFS on metal sites, such as the $\mathrm{Mn_{12}}$ complex.

To assess the magnetic anisotropy of the ground Kramers doublet of the complex, the corresponding **g** tensor was evaluated within the three structural models for the cobalt fragments. The results are listed in Table 10. We can see that in all of the approximations, the obtained **g** tensor is very anisotropic, which stems from the strong magnetic anisotropy of the Co(II) sites. Because of the inversion relation between marginal Co(II) sites, their main magnetic axes are parallel (Figure 5), and thus, their contributions to the **g** tensor of the whole complex are net additive. As a result, the main magnetic axis of the complex (the Z axis) makes an angle of only ~5° with the corresponding main magnetic axes of the marginal Co(II) ions (Figure 5). The saturation magnetization along the main magnetic axis is $^1/_2 g_Z \mu_B = 10.1\mu_B$.

Why the $[\mathrm{Co^{II}_3Co^{III}_4(L)_6(MeO)_6}]$ Complex Is Not an SMM. Finally, the obtained ab initio results provide an understanding of why SMM behavior is not observed for the $[\mathrm{Co^{II}_3Co^{III}_4(L)_6(MeO)_6}]$ complex. In SMMs such as the $\mathrm{Mn_{12}}$ and $\mathrm{Fe_8}$ complexes at temperatures low enough that only the lowest doublet ($\pm S$) of the ground spin multiplet S split by the axial magnetic anisotropy (eq 1) is populated, the magnetic relaxation becomes temperature-independent.[68,69] Its rate was found to be proportional to the square of the tunneling matrix element Δ, which determines the tunneling splitting of the lowest doublet.[70] It is clear that the complex can become an SMM only for small enough values of Δ, on the order of 10^{-8} cm^{-1} for the $\mathrm{Fe_8}$ complex and 10^{-10} cm^{-1} for the $\mathrm{Mn_{12}}$ complex.[1b,70] Since both of these complexes are characterized by integer spin ($S = 10$ in the ground state), the main contribution to the splitting parameter Δ at low temperature comes from the rhombic anisotropy term $E(\hat{S}_x^2 - \hat{S}_y^2)$ and higher-order anisotropy terms. On the contrary, the complex $[\mathrm{Co^{II}_3Co^{III}_4(L)_6(MeO)_6}]$ has an odd number of electrons, and its electronic ground state corresponds to a Kramers doublet which, according to the Kramers theorem, cannot be split by any internal interactions. It can, however, be split by an externally applied magnetic field. In order to induce tunneling between the two states ψ_1 and ψ_2 of the ground Kramers doublet, corresponding to saturation (maximal) magnetization in opposite directions, the applied field should have transverse components H_X and H_Y perpendicular to the main magnetic axis Z (Figure 5). The corresponding Zeeman Hamiltonian has the following form:

$$\hat{H}^{\perp}_{\mathrm{Zee}} = -\hat{\mu}_X H_X - \hat{\mu}_Y H_Y \quad (3)$$

where $\hat{\mu}_X$ and $\hat{\mu}_Y$ are magnetic momentum operators along the two transverse magnetic axes of the complex (see Figure 5). The Kramers doublet components ψ_1 and ψ_2 corresponding to saturation magnetization are found as eigenfunctions of the Zeeman interaction for a field applied along the main magnetic axis Z, i.e., they are eigenfunctions of the momentum operator $\hat{\mu}_Z$:

$$\langle \psi_1 | \hat{\mu}_z | \psi_1 \rangle = 10.1\mu_B$$

$$\langle \psi_2 | \hat{\mu}_z | \psi_2 \rangle = -10.1\mu_B$$

$$\langle \psi_1 | \hat{\mu}_z | \psi_2 \rangle = 0.0\mu_B$$

The tunneling parameter corresponding to the Zeeman interaction (eq 3) is simply the modulus of the off-diagonal matrix element of $\hat{H}^{\perp}_{\mathrm{Zee}}$ involving these wave functions:

$$\Delta = |w|, \; w = \langle \psi_1 | \hat{H}^{\perp}_{\mathrm{Zee}} | \psi_2 \rangle \quad (4)$$

According to eq 3, Δ is nonzero only when the matrix elements of the transverse momenta, $\langle \psi_1 | \hat{\mu}_X | \psi_2 \rangle$ and $\langle \psi_1 | \hat{\mu}_Y | \psi_2 \rangle$, are nonzero. The calculated values of these matrix elements are quoted in Table 11. We can see that they are nonzero and relatively large in all of the structural approximations. As a result, any internal magnetic field having a transverse component on the anisotropy axis of the complex, for instance, a field generated by neighboring nuclei or other magnetic molecules, will induce tunneling splitting of the states ψ_1 and ψ_2. There are two sources of internal magnetic fields: dipolar fields from nuclear spins and from the magnetic moments of other molecules in the crystal. The intensities of these fields are within the ranges 1−10 and 10−30 mT, respectively,[1b] for nearest-neighbor groups. Using a field intensity of 1 mT, we calculated the tunneling parameter for the case when the field is applied along the Y direction (Table 11). The values obtained for Δ were 3−4 orders of magnitude larger than the ones for the $\mathrm{Fe_8}$ and $\mathrm{Mn_{12}}$ SMMs quoted above. Since this parameter enters the expression for the rate of magnetic relaxation (τ) as Δ^2,[70] we may conclude that no slow magnetic relaxation behavior is expected in this case, assuming that the other factors governing this relaxation (interaction with the environment) are unchanged.

As the temperature increases, the relaxation time of an SMM gradually becomes temperature-dependent, and starting from a certain value lower than the blocking temperature, the dependence becomes an activated-type dependence for most SMM.[1] The activation energy in the Arrhenius law is actually smaller than the difference between the lowest and the highest levels of the Hamiltonian in eq 1 because at some point the degenerate pairs $\pm M_S$ corresponding to excited levels become strongly split by other interactions. In the case of the $[\mathrm{Co^{II}_3Co^{III}_4(L)_6(MeO)_6}]$ complex, the components of the ground Kramers doublet are already shortcut by the Zeeman interaction: the off-diagonal matrix elements of the transverse magnetic moment are only 1 order of magnitude smaller than those of a free $S = {}^1/_2$ spin. Therefore, even if the matrix elements of the transverse magnetic moment between ψ_1 (or ψ_2) and the components of excited Kramers doublets are much larger, we cannot associate the three excited Kramers doublets in the right-hand side of Figure 7 with a barrier of blockage of magnetization.

The fact that the $\mathrm{Co_7}$ wheel investigated here is not an SMM is surprising at a first glance. Indeed, the exchange interaction in this complex is ferromagnetic, and the magnetic anisotropy on the cobalt sites is overall negative, leading to a large magnetic moment value of $10\mu_B$ in the ground state. However, since the exchange interaction takes place only between the Co(II) ions on the diagonal of the wheel (Figure 5), the symmetry of the resulting Kramers doublets is much lower than the apparent

---

(68) Sangregorio, C.; Ohm, T.; Paulsen, C.; Sessoli, R.; Gatteschi, D. *Phys. Rev. Lett.* **1997**, *78*, 4645–4648.

(69) Thomas, L.; Caneschi, A.; Barbara, B. *Phys. Rev. Lett.* **1999**, *83*, 2398–2401.

(70) Prokof'ev, N. V.; Stamp, P. C. E. *Phys. Rev. Lett.* **1998**, *80*, 5794–5797.

Table 11. Values of the Matrix Elements of the Magnetic Dipole Moment Operators $\hat{\mu}_X$ and $\hat{\mu}_Y$ between States with Saturation Magnetization in the $[Co^{II}_3Co^{III}_4(L)_6(MeO)_6]$ Complex and of the Tunneling Matrix Element Δ, Calculated for the Three Structural Approximations

	A	B	C
$\langle\psi_1|\hat{\mu}_X|\psi_2\rangle/\mu_B$	0.0416 − 0.1319i	−0.0396 + 0.1841i	−0.0308 − 0.0301i
$\langle\psi_1|\hat{\mu}_Y|\psi_2\rangle/\mu_B$	0.1718 + 0.0542i	−0.0318 − 0.0649i	0.0465 − 0.0475i
$\Delta(H_Y = 1\text{ mT})\ (\text{cm}^{-1})$	8.4104×10^{-5}	3.3741×10^{-5}	3.1033×10^{-5}

symmetry of the complex (S_6) and is actually close to orthorhombic. Therefore, it is interesting to compare $[Co^{II}_3Co^{III}_4(L)_6(MeO)_6]$ with the Fe_8 complex,[1b] which is an SMM with a relatively high barrier for reversal of magnetization but also has a geometry that is close to orthorhombic. The orthorhombic symmetry of the Fe_8 complex makes both axial (eq 1) and rhombic anisotropy terms relevant, with a non-negligible ratio of the rhombic (E) and axial (D) parameters ($|E/D| = 0.15-0.19$ for the ground exchange term $S = 10$).[1b] However, this complex is of the strong-exchange-limit type, with eigenstates described to a good approximation by solutions of the Heisenberg-exchange Hamiltonian characterized by a total spin S that are also eigenstates of the axial magnetic anisotropy interaction (eq 1). For such states, the rhombic term $E(\hat{S}_x^2 - \hat{S}_y^2)$ is a perturbation that connects the ±10 components of the ground-state doublet only in the tenth order of perturbation theory, leading to a tunneling splitting between them on the order of $E(E/D)^{10}$.[71] Therefore, the effect of this perturbation will be very strongly reduced for the lowest doublets of the Fe_8 complex. The main conclusion of our study is that the Co_7 wheel is found in the weak-exchange limit, where the spin−orbit splitting of local electronic states on cobalt sites is much stronger than the exchange interaction between the sites. Therefore the criteria for SMM behavior (in particular, eq 1) identified for complexes in the strong-exchange limit, such as Mn_{12} or Fe_8, are not applicable here. It is clear also that the lowering of symmetry has a more pronounced effect on SMM behavior for complexes in the weak-exchange limit than for those in the strong-exchange limit.

Conclusions

In this paper we have presented the synthesis, crystal structure, and magnetic behavior of the heptanuclear wheel $[Co^{II}_3Co^{III}_4(L)_6(MeO)_6]$ together with the first detailed ab initio investigation of its magnetic behavior. The measured magnetic susceptibility evidenced the overall predominance of ferromagnetic interactions between magnetic centers, while micro-SQUID measurements on single crystals showed that this heptanuclear complex is not a single-molecule magnet. The lowest spin states and spin−orbit multiplets of each mononuclear cobalt fragment were investigated using CASSCF/CASPT2/SO-RASSI quantum-chemistry calculations in different structural approximations. The four Co(III) ions were found to be diamagnetic but to give a significant TIP contribution to the susceptibility because of strong magnetic admixture of low-lying excited states. The crystal-field splitting of the lowest terms on three Co(II) sites was found to be comparable to the spin−orbit coupling constant of the cobalt ion. This led to large separations (∼200 cm^{-1}) of the ground Kramers doublets on these sites from the first excited ones, making their attribution to a parent electronic term impossible. As a result, the Co_7 wheel was found to be in a weak-exchange limit, where the lowest electronic states of the complex are adequately described by the anisotropic exchange interaction between the lowest Kramers doublets on the Co(II) sites rather than by their $S = {}^3/_2$ spins. The simulation of exchange interaction was done within the Lines model while keeping the fully ab initio treatment of magnetic anisotropy effects on individual cobalt fragments and gave a good description of the susceptibility and magnetization with a value of 1.5 cm^{-1} for the nearest-neighbor exchange parameter J_1 and a value of 5.5 cm^{-1} for the next-nearest-neighbor exchange parameter J_2. Such a strong ferromagnetic interaction between distant cobalt ions can arise as a result of low electron-promotion energies in the exchange bridges containing Co(III) ions.

Finally, the lack of SMM behavior in the investigated $[Co^{II}_3Co^{III}_4(L)_6(MeO)_6]$ complex is explained by large matrix elements of the transverse magnetic moments between states of saturation magnetization of the ground Kramers doublet of the complex (as evidenced by our ab initio calculations), which lead to tunneling between these states in the presence of transverse components of external magnetic fields. Estimates of the resulting tunneling parameter for a transverse field of 1 mT (a low estimate for a field due to nuclear spins) gave values that exceed by several orders of magnitude the values of the tunneling parameter for the typical SMMs Mn_{12} and Fe_8. This is presumably the reason why slow relaxation of magnetization is not observed in this compound.

Acknowledgment. The “Région Rhône-Alpes” is gratefully acknowledged for financial support. Instrumental support for magnetic measurements was provided by the “Commissariat à l’Energie Atomique” (CEA) through a “Laboratoire de Recherche Conventioné” (LRC N° DSM-03-31). Single-crystal X-ray diffraction studies were performed at the “Centre de Diffractometrie Henri Longchambon” at Université Claude Bernard Lyon 1. The work of the Belgian team was supported by the Belgian Science Foundation and the Flemish Government under the Concerted Action Scheme. We thank Dr. Wolfgang Wernsdorfer for micro-SQUID measurements.

Supporting Information Available: An X-ray crystallographic file in CIF format, the structural models A and B for the ab initio fragment calculations (Figures 1S and 2S, respectively), spin−orbit energies for the Co(III) fragments (Table S1), simulation of the magnetism of the complex within structural model B (Figure 3S), and the exchange spectrum calculated within the three structural models (Table S2). This material is available free of charge via the Internet at http://pubs.acs.org.

JA8029416

---

(71) Similarly, the order of magnitude of the matrix elements of transverse magnetic momenta are $\sim\mu_B(E/D)^{10}$, i.e., several orders of magnitude smaller than those for the Co_7 wheel in Table 11. As a result, the contribution to the tunneling splitting of the ±10 states from the Zeeman interaction with transverse static dipolar fields present in the crystal will be negligible compared with the contribution from rhombic anisotropy term.